

Accurate Single-Molecule Indicator of Solvent Effects

Yilin Guo,[†] Chen Yang,[†] Chuancheng Jia, and Xuefeng Guo*

Cite This: *JACS Au* 2021, 1, 2271–2279

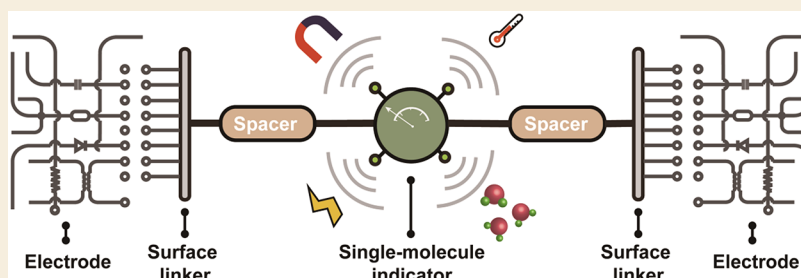
Read Online

ACCESS |

Metrics & More

Article Recommendations

Supporting Information



ABSTRACT: The study of the microscopic structure of solvents is of significant importance for deciphering the essential solvation in chemical reactions and biological processes. Yet conventional technologies, such as neutron diffraction, have an inherent averaging effect as they analyze a group of molecules. In this study, we report a method to analyze the microstructure and interaction in solvents from a single-molecule perspective. A single-molecule electrical nanocircuit is used to directly analyze the dynamic microscopic structure of solvents. Through a single-molecule model reaction, the heterogeneity or homogeneity of solvents is precisely detected at the molecular level. Both the thermodynamics and the kinetics of the model reaction demonstrate the microscopic heterogeneity of alcohol–water and alcohol–*n*-hexane solutions and the microscopic homogeneity of alcohol–carbon tetrachloride solutions. In addition, a real-time event spectroscopy has been developed to study the dynamic characteristics of the segregated phase and the internal intermolecular interaction in microheterogeneous solvents. The development of such a unique high-resolution indicator with single-molecule and single-event accuracy provides infinite opportunities to decipher solvent effects in-depth and optimizes chemical reactions and biological processes in solution.

KEYWORDS: single molecule, solvent microstructure, reaction dynamics, event spectroscopy, molecular electronics

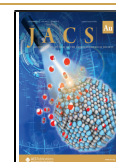
INTRODUCTION

Solvents play an extremely important role in chemical reactions and life processes, whereas the vacuum environment is abhorred by nature. A complete understanding of solvent effects can guide us to decipher the intrinsic mechanism of chemical reactions and life processes, and further to optimize synthetic conditions¹ and regulate the driving force of the biological processes.² For a long time, the understanding and characterization of the solvents can be summarized as (1) intrinsic properties: chemical potential, dipole moment, and dielectric properties; (2) interaction mode (static disorder): hydrogen bond, π - π stacking, hydrophobic interaction, and electrostatic interaction; (3) dynamic properties: diffusion, transfer of charge and energy, etc. These properties have been described by a series of macroscopic-scale solvent experiments, such as solvent thermodynamics,³ diffraction images,⁴ solvatochromism,⁵ etc. However, the most intrinsic characteristics, including solute–solute, solute–solvent, and solvent–solvent interactions, are averaged in these observed macroscopic properties. More local structural features and detailed pictures have never been obtained because of the formidable challenges of direct characterization from a microscopic perspective.

With the rise and flourishing of detection technologies, e.g., optical,^{6,7} mechanical,^{8,9} and electrical^{10,11} methods that are capable of translating the weak signals from individual molecules, single-molecule detection, which reaches the ultimate limit of analytical chemistry, provides intrinsic monitoring of the physical properties and chemical reactions of single molecules under a vacuum and in solution. A variety of external stimuli,¹² such as light,¹³ electric field,^{14,15} temperature,¹⁶ magnetic field,¹⁷ mechanical force,¹⁸ pH,¹⁹ and solvent,^{20,21} can sensitively influence the single-molecule chemical reaction and further approach quantitative regulation. Here, we provide reverse thinking: the intrinsic physical property or chemical reaction of a single molecule with a fixed mode can be used as an indicator to detect subtle changes in the external environment. In this model, the single-molecule active center is seen as a single-molecule indicator and the

Received: September 11, 2021

Published: November 18, 2021



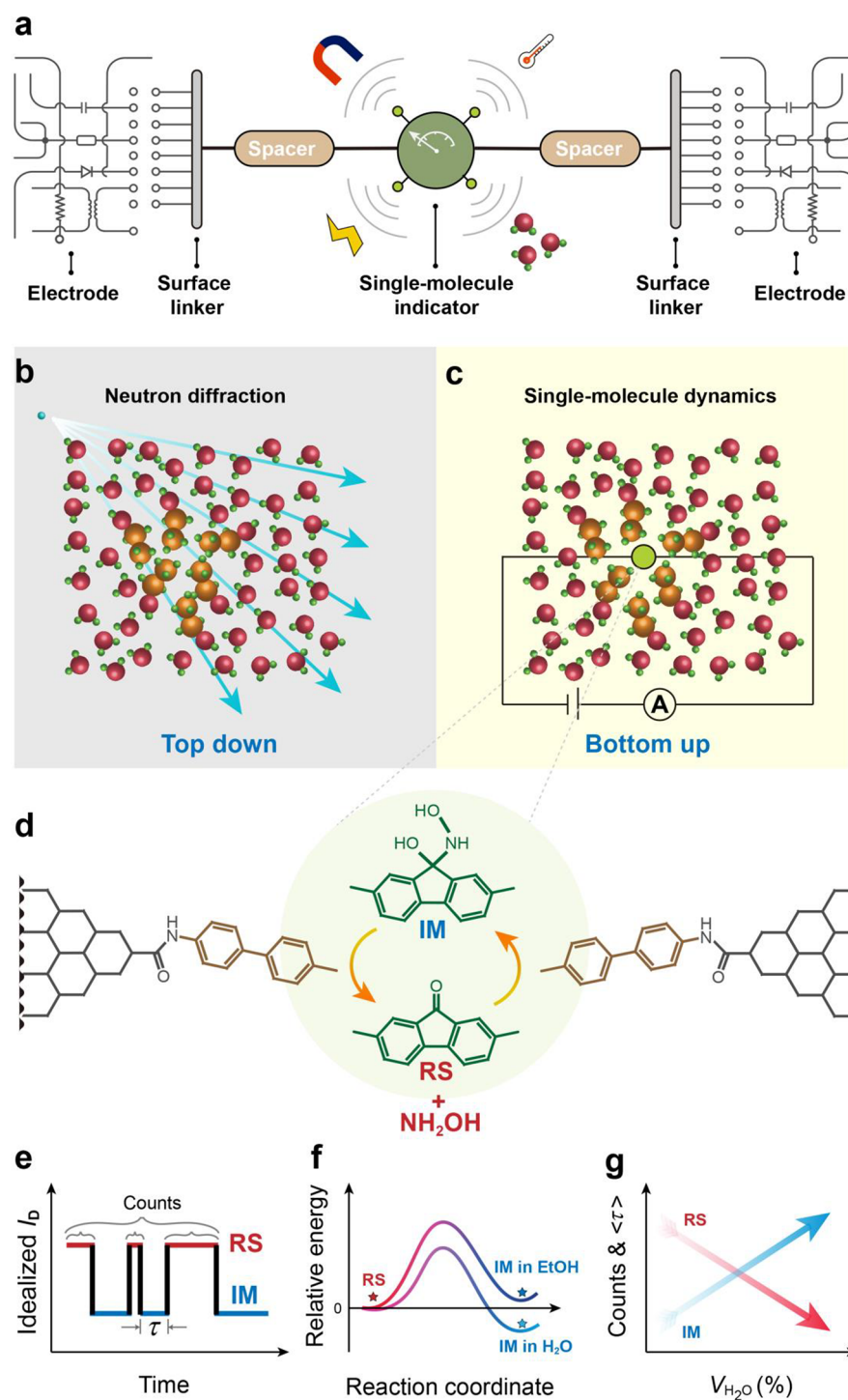


Figure 1. Schematic of a single-molecule model reaction to detect solvent effects. (a) Schematic of a single-molecule electrical platform that responds to external stimuli. (b) Schematic of macroscopic neutron diffraction to detect the microstructure of solvents. (c) Schematic of a single-molecule device to detect the microstructure of solvents. (d) Schematic of the model reaction used in a single-molecule device. The light green circle shadow shows the functional center to highlight the reversible nucleophilic addition reaction. (e) Idealized $I-t$ curve and assignment of the conductance to the corresponding species. (f) Energy profile of the two species in different solvents. (g) Schematic plot of thermodynamics and kinetics versus the proportion of polar component.

surrounding label-free solvent molecules can be detected in detail. While reaching the limit of spatial resolution, time resolution is also important for studying the evolution of the microscopic system. Therefore, among different single-molecule detection methods, the electrical approach is particularly attractive because of its distinct advantages of the

highest time resolution and nondestructive monitoring. The basic idea is that the single-molecule indicator can be integrated into source and drain electrodes with the linker to eliminate the strong coupling from the electrodes. Correspondingly, the influence of external stimuli on the indicator can be clearly reflected in the current signal as shown in Figure 1a.

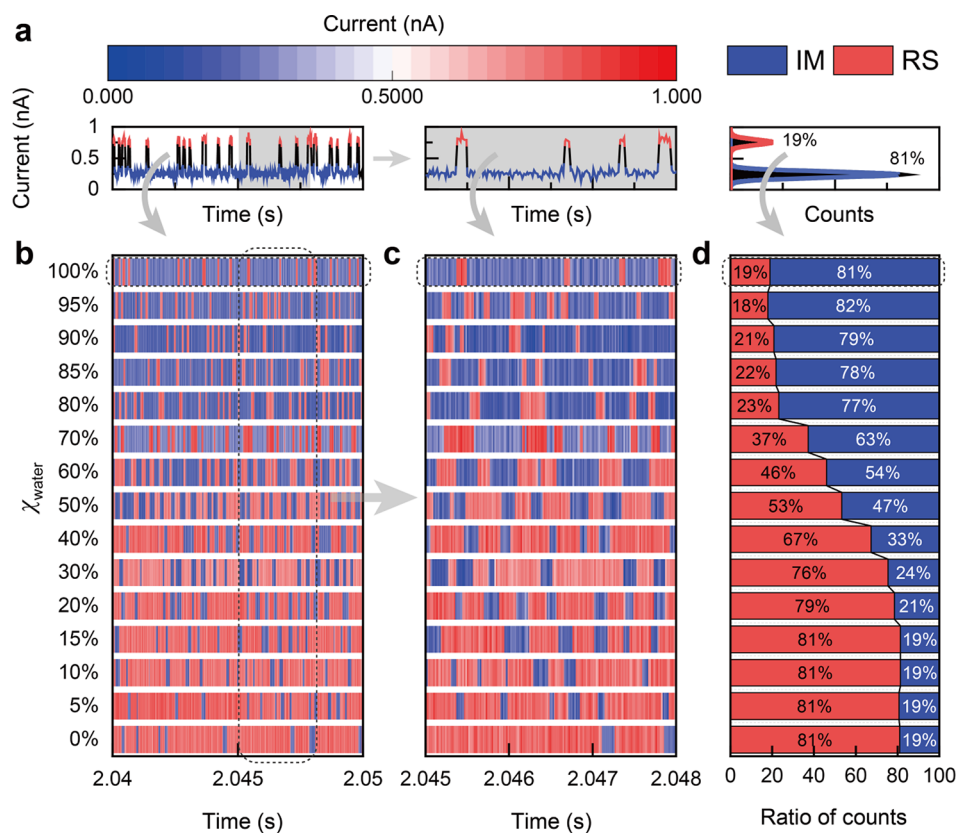


Figure 2. Current signals and thermodynamics in polarity-dependent measurements. (a) $I-t$ curves, corresponding enlarged images and corresponding histograms of the nucleophilic addition reaction in water. (b) Mapping of normalized $I-t$ curves in an ethanol–water solvent with different molar fractions. (c) Corresponding enlarged image of b. (d) Corresponding statistical proportion of two species.

The microscopic heterogeneity of an alcohol–water solution has been extensively studied in recent years. The structure with nonideal (incomplete) mixing of two components at the molecular level has been characterized by combining theoretical molecular dynamics simulations²² or experimental neutron diffraction with isotope substitution^{4,23} or Raman scattering²⁴ (Figure 1b), which suggests the formation of isolated alcohol microscopic micelles at $\chi_{\text{alcohol}}/\chi_{\text{water}} \lesssim 3/7$, isolated hydrogen-bond water clusters at $\chi_{\text{alcohol}}/\chi_{\text{water}} \gtrsim 7/3$, and a bipercolating system at $\sim 3/7 < \chi_{\text{alcohol}}/\chi_{\text{water}} \lesssim 7/3$, where χ is the corresponding mole fraction. Some other solutions, such as amide²⁵ and DMSO²⁶ aqueous solutions, have also been pointed out to have microheterogeneity. This top-down experimental method infers the static microstructure of the solution by measuring the position information among the labeled elements or the strength of the hydrogen bond. However, detailed specific microscopic pictures and dynamic information have never been reported because of the unavailability of a noninvasive high-resolution measurement method from the bottom. In this study, we present a bottom-up strategy to realize the characterization of both the solvation of a single molecule and the solvent microstructure (Figure 1c). A single solvent molecule has been shown to provide solvation, and with an increase in solvent molecules,²⁷ solvation gradually shows a macroscopic property. Therefore, in the case of single-molecule solutes, the subtle structural changes of surrounding solvent molecules can be snapshotted by the highly sensitive electrical platform, which can synchronize the solvent microstructure by monitoring the current signal in real time. To this end, we use the previously

well-studied nucleophilic addition²⁰ as a model reaction because of its obvious solvent dependence (Figure 1d).

EXPERIMENTAL SECTION

Fabrication of Graphene Field-Effect Transistors (FETs)

The pretreated copper sheet (25 μm) was annealed in a hydrogen atmosphere ($16 \text{ cm}^3 \text{ min}^{-1}$) for 1.5 h at 1043 $^\circ\text{C}$. The hydrogen flow was then reduced to $8 \text{ cm}^3 \text{ min}^{-1}$ and methane ($1.6 \text{ cm}^3 \text{ min}^{-1}$) was used as a carbon source to grow graphene on copper sheets. PMMA950 was spin-coated on the copper-based graphene and graphene was transferred to the PMMA film through etching the copper substrate with a FeCl_3 solution. The graphene film was washed successively through a HCl solution and deionized water, and then transferred to a 1.5 cm \times 1.5 cm silicon wafer with 3000 \AA SiO_2 (precleaned via a piranha solution). After 1 h of annealing under a hydrogen atmosphere ($600 \text{ cm}^3 \text{ min}^{-1}$), the PMMA was removed (Figure S1).

The preparation of graphene FETs mainly includes three steps of photolithography and two steps of thermal evaporation. First, the gold marks were deposited on the SiO_2/Si substrate covered with graphene by photolithography and thermal evaporation; then, through photolithography and oxygen plasma etching, the graphene strip with a width of 40 μm was obtained; finally, 80 \AA Cr and 800 \AA Au were evaporated as electrodes by photolithography and thermal evaporation. Additionally, 400 \AA SiO_2 was evaporated on the electrodes to prevent current leakage in the liquid phase. Afterward, the photoresist was removed with acetone to obtain a graphene FET (Figure S1).

Fabrication of Single-Molecule Devices

On the basis of the dashed-line lithography (DLL), the graphene electrode arrays with carboxyl terminals were obtained by electron beam lithography (EBL), oxygen plasma etching, and electrical burning. The graphene point electrode array devices, the molecular

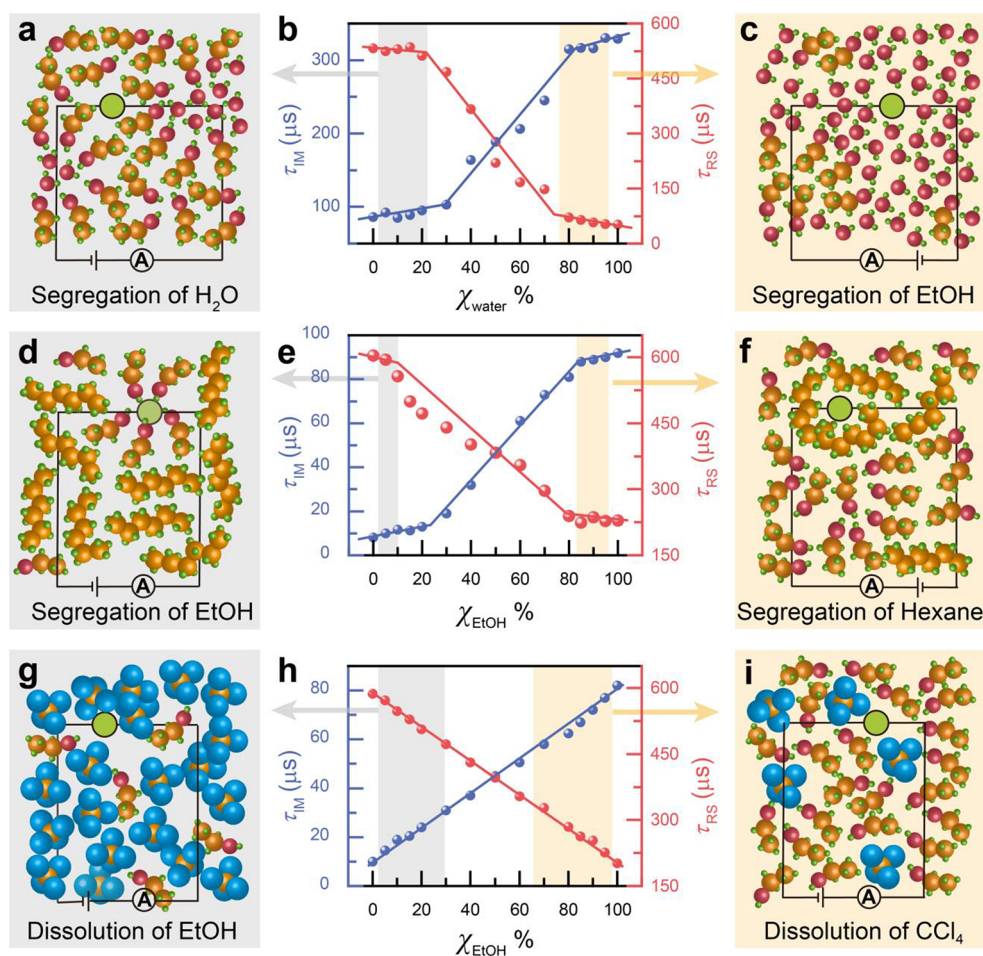


Figure 3. Anomalous kinetics and corresponding schematic of the microscopic structure in mixed solvents. In the case of an ethanol–water solution: (a) Schematic of the segregation of water; (b) plot of the dwell time versus the molar fraction of water; (c) schematic of the segregation of ethanol. In the case of an ethanol–*n*-hexane solution: (d) schematic of the segregation of ethanol; (e) plot of the dwell time versus the molar fraction of ethanol; (f) schematic of the segregation of *n*-hexane. In the case of an ethanol–carbon tetrachloride solution: (g) schematic of the miscibility in a carbon tetrachloride-rich solution; (h) plot of the dwell time versus the molar fraction of ethanol; (i) schematic of the miscibility in an ethanol-rich solution.

bridge (0.1 mM) with amino terminals, the dehydrating agent 1-ethyl-3-(3-(dimethylamino)propyl) carbodiimide (EDCI, 0.1 mM), and 10 mL of pyridine were added to a round-bottom flask under anhydrous and anaerobic conditions. After 48 h, with the catalysis of the dehydrating agent, the amino group at the terminals of the molecular bridge can undergo a dehydration condensation reaction with the carboxyl group at the terminals of the graphene point electrode to form an amide bond. Finally, the single-molecule device was taken out, rinsed with deionized water, and dried with flowing N_2 (Figure S2).

Electrical Characterization

The I – V curves were carried out by an Agilent 4155C semiconductor parameter system and Karl Suss (PMS) manual probe station. The electrical measurements (I – t curves) were measured in the vacuum cryogenic probe station (Lakeshore TTPX). The bias voltages were applied via the auxiliary output of the UHFLI lock-in amplifier. The corresponding electrical signals were amplified by a DHPCA-100 preamplifier and recorded by a NIDAQ high-speed acquisition card at a sampling rate of 439.5 kSa/s.

Characterization of Single-Molecule Junctions

To characterize the single-molecules connection, we first measured the I – V curves of the device after the oxygen plasma etching. No response of the current versus bias voltage was recorded, indicating an open circuit (red curve in Figure S3). After the integration of the

molecular bridge, the current recovered to some extent (blue curve in Figure S3).

RESULTS AND DISCUSSION

Ethanol–Water Solution

In a solution environment at room temperature, the reaction center reversibly reacts with NH_2OH (10 μM) and shows binary switching between two conductance states. According to previous experimental results and theoretical studies,²⁰ we can assign the fluorenone reactant state (RS) to the high conductance and the intermediate (IM) after addition to the low conductance (Figure 1e). The switching conductance states can be recorded in real time to monitor the progress of the reaction. RS and IM have a converse preference to the solvent polarity: In general, IM tends to exist stably in high-polarity solvents like water while RS to low-polarity solvents such as ethanol (Figure 1f). As the polarity of the solvent increases, the dwell time τ (kinetics) of IM gradually increases and contributes to a major proportion of conductance states (thermodynamics) (Figure 1g). These reflect the sensitivity of single-molecule chemical reactions to the solvent environment. In addition, control experiments in Figure S4 excluded the participation of solvents in the reaction. However, these

properties do not vary completely linearly as shown in Figure 1g at low molar fraction ranges such as ($\chi_{\text{water}} < 20\%$ or $\chi_{\text{water}} > 80\%$),²⁰ which implies the nonideal mixed solution environment and more in-depth information that deserve further exploration.

First, we carried out the refined measurements at the low molar fraction range and counted the proportions of RS and IM. Normalized $I-t$ curves (10 ms) under different solvent polarities were displayed by mapping (Figure 2a), and other long-term data and statistics results are provided in Figures S5–S7. As the molar fraction of water increased, we found that the color of the two-dimensional graph gradually becomes blue (Figure 2b), which means that the proportion of low-conductance states (IM) increases and is consistent with the previous experimental results. By comparing the zoom-in images (Figure 2c) of each solvent environment, we can easily find that as the polarity of the solvent increases, the dwell time of the two species shows an opposite trend. Furthermore, we counted the proportions of the two conductance states (Figure 2d) and found that the change in solvent compositions has no significant effect on the thermodynamics of the reaction (Figure 2d) at the two low molar fraction ranges. In the case of $\chi_{\text{water}} < 20\%$, the proportion stays at $\sim 21:79$, whereas it stays at $\sim 81:19$ when $\chi_{\text{water}} > 80\%$, which implies the nonideality of mixed solvents in thermodynamics. Macroscopically, it appears to have less solution mixing entropy than expected (negative excess entropy, ΔS^E). The $|\Delta S^E|$ increased when the small components were added either in the water-rich or ethanol-rich systems, until the extreme value at a 1:1 mixture was reached, which was consistent with the lower slope in both sides of Figure 3b. In other words, the slope in the dwell time–composition diagram has an anticorrelation with the change rate (the first derivative values) of ΔS^E to some extent. This shows the thermodynamic characterization of nonideal solutions with single-molecule insight.

In the case of kinetics, the dwell times of the two species can be extracted and displayed as a single exponential fitting, respectively, to obtain their lifetimes (the fixed concentration of NH_2OH in different systems can rule out its influence on the dwell time of the two species) (Figures S8–S10). The lifetimes of the two species in an ethanol–water solution environment with the gradient molar fraction are shown in Figure 3a–c. A nonlinear trend was found in lifetime versus molar fraction: Two low molar fraction regions exhibited relative insensitivity to changes in solvent composition compared to the solution with $\chi_{\text{water}} = 20\text{--}80\%$, which implies that the properties of the $\chi_{\text{water}} < 20\%$ solution are more like those of ethanol, whereas those of the $\chi_{\text{water}} > 80\%$ solution are more like the properties of water. According to previous studies on this system,⁴ we believe that this phenomenon results from the segregation of water or ethanol in the solution. In an alcohol-rich solution, because of the repulsive interaction between the alcohol alkyl tails and water and the hydrogen-bond interaction among the alcohol hydroxyl heads and water, the water molecules exist as clusters and are surrounded by the ethanol hydroxyl heads in the fluid of ethyl groups (Figure 3a).^{4,28,29} Although the mixing model is unfavorable for entropy increase, the decrease in enthalpy through the formation of a hydrogen-bond network reduces the overall potential energy of the solution. On the contrary, in a water-rich solution, ethanol always tends to stack alkyl tails inside and form hydrophobic interactions (Figure 3c). The hydroxyl heads are exposed to the outside and form a hydrogen bond

with water to form a micromicelle structure. In these two cases, because of the segregation of low molar fraction components in the solvent, the single-molecule reaction is almost solvated by the dominant component in the solution and leads to three ranges of reaction kinetics when χ_{water} changes from 0 to 100% (Figure 3b). Note that the existence of the azeotrope (resulting from the deviation of Raoult's law), the variations in the partial molar volume, and the negative ΔS^E in the macroscopic experiments all show the nonideality of the mixed solution. A detailed understanding about the intermolecular interaction, the three-dimensional hydrogen-bond network, and the microscopic structure have been built with the corresponding evidence, such as high precision microcalorimeters, scattering methods, and theoretical studies.³⁰

Nonaqueous System

On the basis of this strategy, the segregation and phase separation of other aqueous solutions at the molecular level can be measured through the same single-molecule electrical platform. For example, the mixed system of methanol and water shows similar results as the ethanol–water system and the details are provided in Figures S11–S16. Furthermore, we measured the nonaqueous system. In the mixed solution of ethanol and *n*-hexane, the statistic results of $I-t$ curves (Figures S17–S19) also showed nonideality in thermodynamics. We further calculated the lifetimes of the two species under these gradient solvent environments and found that IMs are shorter than in the alcohol–water system, which means that the equilibrium is shifted to the left (Figures S20–S22). The lifetimes of these two species versus solvent component were plotted in Figure 3d–f and showed the three-range distribution. It is not difficult to understand that the low molar fraction of *n*-hexane prefers to avoid the interaction with hydroxyl heads of ethanol and tend to have hydrophobic interactions with the ethanol alkyl tails³¹ (Figure 3d), whereas the low molar fraction of ethanol is prone to spontaneously interact with itself through hydrogen-bond interactions, exposing the alkyl tails to the outside to form a hydrophobic interaction with *n*-hexane (Figure 3f). Similarly, the system of a carbon tetrachloride–ethanol solution disfavored the high-polarity of IMs and contributed to a left equilibrium (Figures S23–S28). However, similar analysis of the kinetics versus the component shows a linear relationship (Figure 3g–i), indicating an approximately ideal mixing and no segregation (homogeneity) in the solution. This can be explained by the formation of C–Cl \cdots O and Cl \cdots H–O atomic quadrupolar interaction.³² Accordingly, the affinity between carbon tetrachloride and ethanol is greater than that among themselves, leading to a mixed solution at the molecular scale. In addition, different from the chain (stick)-like systems (alcohol–water and alcohol–*n*-hexane), the tetrahedral structure of CCl_4 may have more degrees of freedom to interact with alcohol, which leads to an “approximately ideal mixing”. This solution can also be a control to prove the accuracy of the single-molecule platform for label-free detection of the solvent environment.

Real-Time Single-Molecule Event Spectroscopy (r-SMES)

The microheterogeneity and homogeneity and corresponding concentration range in a binary liquid system can be distinguished through the single-molecule solvent-dependent experiments. More detailed information hidden in the solvent can also be provided by our single-molecule devices. For example, the effect of ethanol in a water-rich solution on the

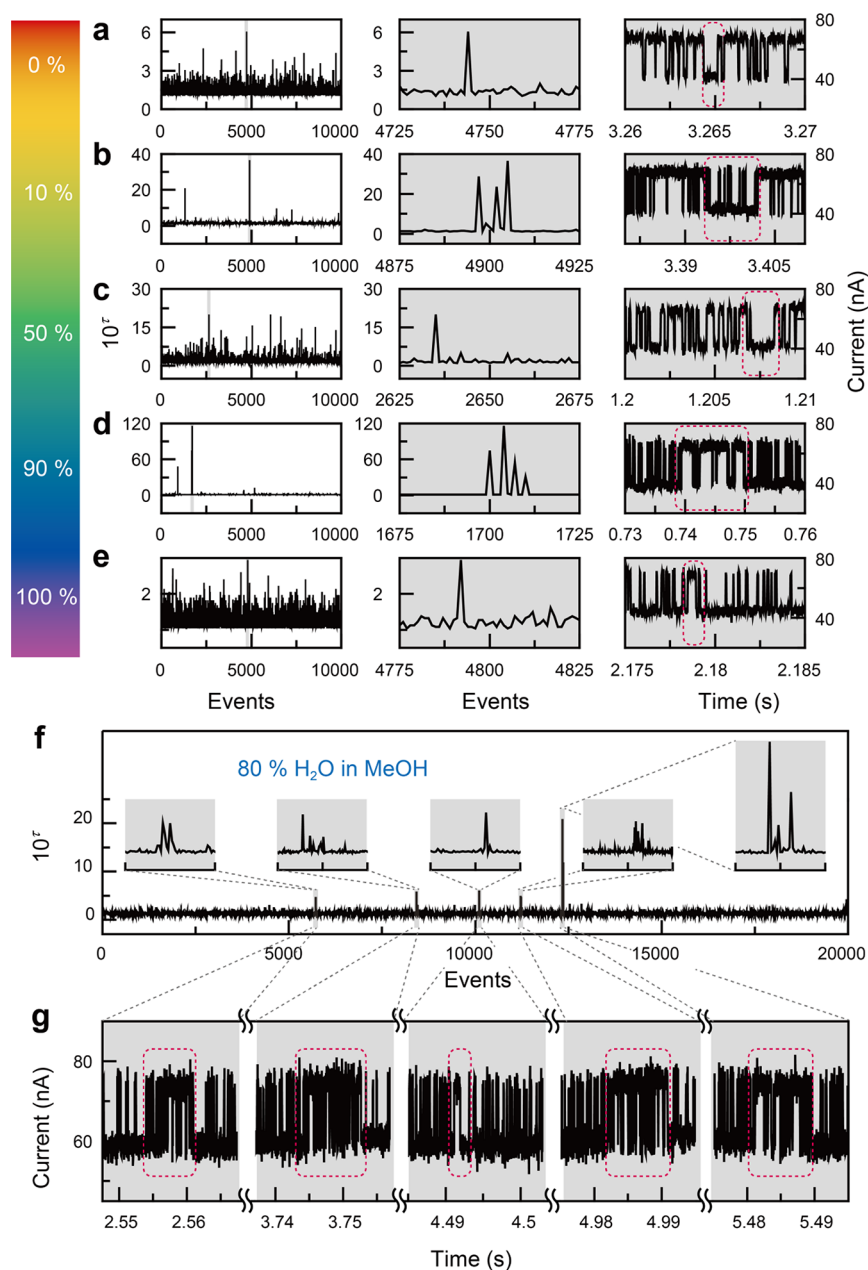


Figure 4. Real-time single-molecule event spectroscopy. (a–e) Spectra, corresponding enlarged peaks, and corresponding time windows of $I-t$ curves in an ethanol solution with $\chi_{\text{water}} =$ (a) 0, (b) 10, (c) 50, (d) 90, and (e) 100%. (f) Real-time event spectra in a methanol solution with $\chi_{\text{water}} = 80\%$. Insets show the corresponding enlarged peaks. (g) Corresponding $I-t$ curves of the peaks in f. The model-switching current curves in the red dashed frame correspond to the enlarged peak in r-SMESs.

single-molecule reaction can be detected. Because of the much faster time scale of a chemical reaction than of diffusion of a separated cluster, the small segregated components have the ability to solvate the reaction center in the single-molecule reaction coordinate and then affect the current signal. During real-time monitoring, the special kinetic properties derived from the current signal could be detected at the moment of segregated component solvation, when they are generally masked by previous single-exponential fitting of the dwell time. Because of the high time resolution, single-event monitoring of the single-molecule reaction can be approached. Therefore, the dwell times of each reaction event were extracted to search for the heterogeneity in the current signal. In the case of ethanol-rich solutions, the relative shorter dwell time of IMs may have

a significant increase with the accidental solvation of water clusters and vice versa. However, in our measurements, because the shortest dwell time is limited to the highest sampling rates of current signals (439.5 kSa/s, $\sim 3 \mu\text{s}$), it is difficult for us to distinguish the significantly reduced dwell time. As for the increased dwell time, we can magnify it exponentially (10^7) and clearly distinguish it in the form of the real-time single-molecule event spectra (r-SMES). r-SMES show the statistics of the dwell time of each event arranged in the order of occurrence within a period of time, which reveals the anomalous behavior in the stochastic process. Therefore, we can detect the increased dwell time of microphase-solvated IMs in ethanol-rich solutions and corresponding RSs in water-rich solutions. We compared the pure solvent, isolated

segregated solution, and 1:1 mixed solution,²³ respectively (Figures 4a–e). For the r-SMES of pure water (Figure 4a) or ethanol (Figure 4e), we zoomed in on the peaks that appeared and found that the peaks were all single peaks (Figure 4a, middle, and Figure 4e, middle), which shows that the abnormally long dwell time results from a single accidental event, as displayed in corresponding $I-t$ curves (Figure 4a, right, and Figure 4e, right). This phenomenon shows that the single-molecule reaction can be treated as a stochastic process and the dwell time can be predicted by the Poisson distribution model. In the case of segregated solutions, the peaks in the r-SMES were all multi-peaks or shoulder peaks, indicating the occurrence of a multiple longer dwell time process at adjacent events (ethanol, Figure 4b; water, Figure 4d), which are very special in the stochastic process. Note that the signal-to-noise ratio (SNR) of the r-SMES in these two cases is higher than that of the pure solvent, indicating that these longer dwell times have a stronger heterogeneity. The corresponding positions in $I-t$ curves were also localized according to the peaks and revealed a reversal of the binary conductance switching during these time intervals, which indicates that the local thermodynamics and kinetics are quite different from the whole reaction process. This phenomenon can be attributed to the continuous solvation process of the segregated component for a certain time interval. For a 1:1 mixed solution of the two components, the r-SMES show a single peak with a small SNR like those of the pure solvents. This phenomenon can be attributed to two main reasons: (1) The solvation from both bulk components. Although the nonideality and the microscopic phase separation exist at any composition (the variations in the partial molar volume exist at all compositions), the influence on the single-molecule indicator from the bulk component was statistically significant. Therefore, the thermodynamic and kinetic parameters obtained via statistics showed properties that are equivalent to those at the macroscopic scale. In addition, the disappearance of the binary conductance switching in the r-SMES can be attributed to the absence of the specificity of solvation (the signal from the solvation of the nanoclusters was submerged in the bulk solvent solvation, leading to an overall stochastic signal). (2) The bipercolation of the two components. The separated microscopic phase at the system has a dynamic disorder, which can be described as “percolation”.²³ Different from the water-rich or ethanol-rich system, both components in the 20–80% molar fraction will percolate throughout the entire solution. Combined with the fast escape and reformation of cluster solvent members, the probability of solvation of the single-molecule indicator by isolated solvent clusters decreased to some extent, leading to the imperceptibility in the r-SMES. The details of r-SMES of ethanol and methanol aqueous solutions are provided in Figures S29–S34. On the basis of this, we can directly determine whether there is micro-heterogeneity in an arbitrary molar fraction mixed solution through the r-SMES.

The analysis of the spatial structure in the solution is equivalent to ergodic long-term statistics at one point. Taking the water–methanol solution with $\chi_{\text{water}} = 80\%$ as an example, each group of multi-peaks in the r-SMES (Figure 4f) and the reverse binary switching of the corresponding $I-t$ curves (Figure 4g) show the real-time change of the microstructure of the solvent at the single-molecule site. Intuitively, we believe that the size of the peak group depends on the spatial scale of the segregated phase and its interaction with the single-

molecule indicator, whereas the frequency of the peak clusters depends on the diffusion rate of the separated phase in the dominated component, i.e., the strength of the interaction between the microphase and the overall solution. The average time ranges (sizes) of the peak groups $\langle\tau_1\rangle \approx 5.69$ ms in the r-SMES indicates the time scales of the interaction (solvation) between the nanoclusters and the single-molecule indicator. The frequency for the methanol nanoclusters leaving from the single-molecule site can be also obtained: $k_{\text{leave}} = 1/\langle\tau_1\rangle \approx 175.5$ s⁻¹, which is positively correlated with its diffusion rate. The average time intervals $\langle\tau_0\rangle \approx 1.24$ s between the peak groups in the r-SMES can be used to evaluate the frequency for the methanol nanoclusters arriving at the single-molecule site: $k_{\text{arrive}} = 1/\langle\tau_0\rangle \approx 0.8$ s⁻¹, which is also positively correlated with the diffusion rate. The difference between these two frequencies mainly results from the spatial factor: there is a lower probability for a nanocluster diffusing to specified single-molecule sites. In addition, these frequencies can also be affected by the dynamic dissociation–reformation process of the nanocluster²³ (favorable with the increase in the entire positional entropy), which leads us to underestimate the measured value.

Furthermore, we chose two kinds of mixed solutions with different interactions, ethanol–water and tetrahydrofuran–water solution at $\chi_{\text{water}} = 80\%$, and compared their r-SMES (Figures S29–S31 and Figure S35). The ethanol–water solution has larger peak groups but longer intervals among themselves, whereas the tetrahydrofuran–water solution shows an opposite property. This reflects the difference in the microscopic spatial structure and interaction mode in the two solutions: ethanol behaves as both the hydrogen-bond donor and acceptor, whereas tetrahydrofuran acts only as an acceptor. The ethanol molecules have a stronger interaction with the single-molecule indicator than tetrahydrofuran and lead to larger peak groups. However, they also have a stronger interaction with water and are trapped in the hydrogen-bond network, thus causing a relatively slow diffusion and a longer interval among peak groups of r-SMES, which agrees with previous works.^{23,31} Based on single-molecule solvation by different solvents, the r-SMES shed light on not only the heterogeneity of the solution but also the internal interactions in the solution. Note that there are some other factors that affect the significance of the current model switching and the r-SMES, such as the short time scale of the transition-state solvation, which cannot be achieved by our sampling rate. Nonetheless, the rise of single-molecule probes³³ gives us confidence that the electrical single-molecule platform is promising to detect the supercritical fluid, microphase transition,³⁴ nucleation mechanism,³⁵ and chemical oscillation systems from single-molecule insight.

CONCLUSIONS

In this work, a unique method for label-free detection of solvent effects is established using a single-molecule electrical platform. The microstructure of several mixed solutions was accurately revealed by a fixed-mode nucleophilic addition reaction. More importantly, we developed real-time single-molecule event spectroscopy to directly detect the microscopic heterogeneity of the solution and compare the interaction in the solvent network. The intermolecular interaction in the alcohol–water, alcohol–*n*-hexane (alkyl tail versus hydroxyl), and alcohol–CCl₄ (C–Cl⋯O and Cl⋯H–O) system were characterized with single-molecule insight. These results

provide novel insights into the detection of the mystery of the microworld from the bottom, which has the potential to deeply understand solvent effects and further regulates chemical reactions and life processes.

■ ASSOCIATED CONTENT

Supporting Information

The Supporting Information is available free of charge at <https://pubs.acs.org/doi/10.1021/jacsau.1c00400>.

Control experiments of different solvents; long-term data and statistical results of water–EtOH, water–MeOH, EtOH–*n*-hexane, and EtOH–CCl₄ mixed solutions; real-time single-molecule event spectroscopy of water–EtOH, water–MeOH, and water–THF solutions (PDF)

■ AUTHOR INFORMATION

Corresponding Author

Xuefeng Guo – State Key Laboratory for Structural Chemistry of Unstable and Stable Species, Beijing National Laboratory for Molecular Sciences, National Biomedical Imaging Center, College of Chemistry and Molecular Engineering, Peking University, Beijing 100871, P. R. China; Center of Single-Molecule Sciences, Frontiers Science Center for New Organic Matter, Institute of Modern Optics, College of Electronic Information and Optical Engineering, Nankai University, Tianjin 300350, P. R. China; orcid.org/0000-0001-5723-8528; Email: guoxf@pku.edu.cn

Authors

Yilin Guo – State Key Laboratory for Structural Chemistry of Unstable and Stable Species, Beijing National Laboratory for Molecular Sciences, National Biomedical Imaging Center, College of Chemistry and Molecular Engineering, Peking University, Beijing 100871, P. R. China

Chen Yang – State Key Laboratory for Structural Chemistry of Unstable and Stable Species, Beijing National Laboratory for Molecular Sciences, National Biomedical Imaging Center, College of Chemistry and Molecular Engineering, Peking University, Beijing 100871, P. R. China

Chuancheng Jia – Center of Single-Molecule Sciences, Frontiers Science Center for New Organic Matter, Institute of Modern Optics, College of Electronic Information and Optical Engineering, Nankai University, Tianjin 300350, P. R. China

Complete contact information is available at: <https://pubs.acs.org/doi/10.1021/jacsau.1c00400>

Author Contributions

X.G. conceived and designed the experiments. Y.G. and C.Y. fabricated the devices and performed the device measurements. X.G., C.J., Y.G., and C.Y. analyzed the data and wrote the paper. All authors discussed the results and commented on the manuscript.

Author Contributions

[†]Y.G. and C.Y. contributed equally to this work.

Notes

The authors declare no competing financial interest.

■ ACKNOWLEDGMENTS

We acknowledge primary financial support from the National Key R&D Program of China (2017YFA0204901), the National Natural Science Foundation of China (21727806 and 21933001), “Frontiers Science Center for New Organic Matter” at Nankai University (63181206), and the Tencent Foundation through the XPLOER PRIZE.

■ REFERENCES

- (1) Adams, J. S.; Chemburkar, A.; Priyadarshini, P.; Ricciardulli, T.; Lu, Y. B.; Maliakkal, V.; Sampath, A.; Winikoff, S.; Karim, A. M.; Neurock, M.; Flaherty, D. W. Solvent molecules form surface redox mediators in situ and cocatalyze O₂ reduction on Pd. *Science* **2021**, *371*, 626–632.
- (2) Discher, D. E.; Eisenberg, A. Polymer vesicles. *Science* **2002**, *297*, 967–973.
- (3) Ratkova, E. L.; Palmer, D. S.; Fedorov, M. V. Solvation thermodynamics of organic molecules by the molecular integral equation theory: Approaching chemical accuracy. *Chem. Rev.* **2015**, *115*, 6312–6356.
- (4) Dixit, S.; Crain, J.; Poon, W. C. K.; Finney, J. L.; Soper, A. K. Molecular segregation observed in a concentrated alcohol–water solution. *Nature* **2002**, *416*, 829–832.
- (5) Fried, S. D.; Boxer, S. G. Measuring electric fields and noncovalent interactions using the vibrational stark effect. *Acc. Chem. Res.* **2015**, *48*, 998–1006.
- (6) Heller, I.; Hoekstra, T. P.; King, G. A.; Peterman, E. J. G.; Wuite, G. J. L. Optical tweezers analysis of DNA–protein complexes. *Chem. Rev.* **2014**, *114*, 3087–3119.
- (7) Zrimsek, A. B.; Chiang, N.; Mattei, M.; Zaleski, S.; McAnally, M. O.; Chapman, C. T.; Henry, A.-I.; Schatz, G. C.; Van Deyne, R. P. Single-molecule chemistry with surface- and tip-enhanced Raman spectroscopy. *Chem. Rev.* **2017**, *117*, 7583–7613.
- (8) Liu, C.; Kubo, K.; Wang, E.; Han, K.-S.; Yang, F.; Chen, G.; Escobedo, F. A.; Coates, G. W.; Chen, P. Single polymer growth dynamics. *Science* **2017**, *358*, 352–355.
- (9) Florin, E. L.; Moy, V. T.; Gaub, H. E. Adhesion forces between individual ligand–receptor pairs. *Science* **1994**, *264*, 415–417.
- (10) Li, Y.; Yang, C.; Guo, X. Single-molecule electrical detection: A promising route toward the fundamental limits of chemistry and life science. *Acc. Chem. Res.* **2020**, *53*, 159–169.
- (11) Howorka, S.; Siwy, Z. Nanopore analytics: Sensing of single molecules. *Chem. Soc. Rev.* **2009**, *38*, 2360–2384.
- (12) Xin, N.; Guan, J.; Zhou, C.; Chen, X.; Gu, C.; Li, Y.; Ratner, M. A.; Nitzan, A.; Stoddart, J. F.; Guo, X. Concepts in the design and engineering of single-molecule electronic devices. *Nat. Rev. Phys.* **2019**, *1*, 211–230.
- (13) Jia, C.; Migliore, A.; Xin, N.; Huang, S.; Wang, J.; Yang, Q.; Wang, S.; Chen, H.; Wang, D.; Feng, B.; Liu, Z.; Zhang, G.; Qu, D.-H.; Tian, H.; Ratner, M. A.; Xu, H. Q.; Nitzan, A.; Guo, X. Covalently bonded single-molecule junctions with stable and reversible photo-switched conductivity. *Science* **2016**, *352*, 1443–1445.
- (14) Yang, C.; Liu, Z.; Li, Y.; Zhou, S.; Lu, C.; Guo, Y.; Ramirez, M.; Zhang, Q.; Li, Y.; Liu, Z.; et al. Electric field–catalyzed single-molecule Diels–Alder reaction dynamics. *Sci. Adv.* **2021**, *7*, eabf0689.
- (15) Aragonès, A. C.; Haworth, N. L.; Darwish, N.; Ciampi, S.; Bloomfield, N. J.; Wallace, G. G.; Diez-Perez, I.; Coote, M. L. Electrostatic catalysis of a Diels–Alder reaction. *Nature* **2016**, *531*, 88–91.
- (16) Xin, N.; Wang, J.; Jia, C.; Liu, Z.; Zhang, X.; Yu, C.; Li, M.; Wang, S.; Gong, Y.; Sun, H.; Zhang, G.; Liu, Z.; Zhang, G.; Liao, J.; Zhang, D.; Guo, X. Stereoelectronic effect-induced conductance switching in aromatic chain single-molecule junctions. *Nano Lett.* **2017**, *17*, 856–861.
- (17) Kim, W. Y.; Kim, K. S. Tuning molecular orbitals in molecular electronics and spintronics. *Acc. Chem. Res.* **2010**, *43*, 111–120.
- (18) Tang, C.; Tang, Y.; Ye, Y.; Yan, Z.; Chen, Z.; Chen, L.; Zhang, L.; Liu, J.; Shi, J.; Xia, H.; Hong, W. Identifying the conformational

isomers of single-molecule cyclohexane at room temperature. *Chem.* **2020**, *6*, 2770–2781.

(19) Darwish, N.; Aragonès, A. C.; Darwish, T.; Ciampi, S.; Díez-Pérez, I. Multi-responsive photo- and chemo-electrical single-molecule switches. *Nano Lett.* **2014**, *14*, 7064–7070.

(20) Guan, J.; Jia, C.; Li, Y.; Liu, Z.; Wang, J.; Yang, Z.; Gu, C.; Su, D.; Houk, K. N.; Zhang, D.; Guo, X. Direct single-molecule dynamic detection of chemical reactions. *Sci. Adv.* **2018**, *4*, eaar2177.

(21) Gu, C.; Hu, C.; Wei, Y.; Lin, D.; Jia, C.; Li, M.; Su, D.; Guan, J.; Xia, A.; Xie, L.; Nitzan, A.; Guo, H.; Guo, X. Label-free dynamic detection of single-molecule nucleophilic-substitution reactions. *Nano Lett.* **2018**, *18*, 4156–4162.

(22) Mallamace, F.; Corsaro, C.; Mallamace, D.; Vasi, C.; Vasi, S.; Stanley, H. E. Dynamical properties of water-methanol solutions. *J. Chem. Phys.* **2016**, *144*, 064506.

(23) Dougan, L.; Bates, S. P.; Hargreaves, R.; Fox, J. P.; Crain, J.; Finney, J. L.; Reat, V.; Soper, A. K. Methanol-water solutions: A bi-percolating liquid mixture. *J. Chem. Phys.* **2004**, *121*, 6456–6462.

(24) Ratajska-Gadomska, B.; Gadomski, W. Influence of confinement on solvation of ethanol in water studied by Raman spectroscopy. *J. Chem. Phys.* **2010**, *133*, 234505.

(25) Salamatova, E.; Cunha, A. V.; Bloem, R.; Roeters, S. J.; Woutersen, S.; Jansen, T. L. C.; Pshenichnikov, M. S. Hydrophobic collapse in N-methylacetamide-water mixtures. *J. Phys. Chem. A* **2018**, *122*, 2468–2478.

(26) Soper, A. K.; Luzar, A. A neutron diffraction study of dimethyl sulfoxide–water mixtures. *J. Chem. Phys.* **1992**, *97*, 1320–1331.

(27) Otto, R.; Brox, J.; Trippel, S.; Stei, M.; Best, T.; Wester, R. Single solvent molecules can affect the dynamics of substitution reactions. *Nat. Chem.* **2012**, *4*, 534–538.

(28) Noskov, S. Y.; Lamoureux, G.; Roux, B. Molecular dynamics study of hydration in ethanol-water mixtures using a polarizable force field. *J. Phys. Chem. B* **2005**, *109*, 6705–6713.

(29) Matsumoto, M.; Nishi, N.; Furusawa, T.; Saita, M.; Takamuku, T.; Yamagami, M.; Yamaguchi, T. Structure of clusters in ethanol-water binary-solutions studied by mass-spectrometry and X-ray-diffraction. *Bull. Chem. Soc. Jpn.* **1995**, *68*, 1775–1783.

(30) Franks, F.; Desnoyers, J. E. Alcohol–water mixtures revisited. In *Water Science Reviews*; Cambridge University Press, 1989; Vol. 1, pp 171–232.

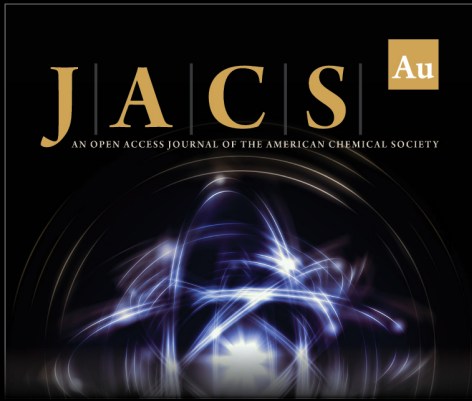
(31) Jukic, I.; PoZar, M.; Lovrinevic, B. Comparative analysis of ethanol dynamics in aqueous and non-aqueous solutions. *Phys. Chem. Chem. Phys.* **2020**, *22*, 23856–23868.

(32) Torii, H. Atomic quadrupolar effect in the methanol–CCl₄ and water–CCl₄ intermolecular interactions. *Chem. Phys. Lett.* **2004**, *393*, 153–158.

(33) Shen, B.; Chen, X.; Wang, H.; Xiong, H.; Bosch, E. G. T.; Lazić, I.; Cai, D.; Qian, W.; Jin, S.; Liu, X.; Han, Y.; Wei, F. A single-molecule van der Waals compass. *Nature* **2021**, *592*, 541–544.

(34) Kim, K. H.; Amann-Winkel, K.; Giovambattista, N.; Spah, A.; Perakis, F.; Pathak, H.; Parada, M. L.; Yang, C.; Mariedahl, D.; Eklund, T.; Lane, T. J.; You, S.; Jeong, S.; Weston, M.; Lee, J. H.; Eom, I.; Kim, M.; Park, J.; Chun, S. H.; Poole, P. H.; Nilsson, A. Experimental observation of the liquid-liquid transition in bulk supercooled water under pressure. *Science* **2020**, *370*, 978–982.

(35) Erdemir, D.; Lee, A. Y.; Myerson, A. S. Nucleation of crystals from solution: Classical and two-step models. *Acc. Chem. Res.* **2009**, *42*, 621–629.



JACS Au
AN OPEN ACCESS JOURNAL OF THE AMERICAN CHEMICAL SOCIETY

Editor-in-Chief
Prof. Christopher W. Jones
Georgia Institute of Technology, USA

Open for Submissions 

pubs.acs.org/jacsau  ACS Publications
Most Trusted. Most Cited. Most Read.